Journal of Solid State Chemistry 184 (2011) 246–251

Contents lists available at ScienceDirect

Journal of Solid State Chemistry

journal homepage: www.elsevier.com/locate/jssc

Polyol-mediated solvothermal synthesis and luminescence properties of CeF_3, and CeF_3:Tb^{3+} nanocrystals

Xuesong Qu [a,b], Hyun Kyoung Yang [a], Jong Won Chung [a], Byung Kee Moon [a], Byung Chun Choi [a], Jung Hyun Jeong [a,*], Kwang Ho Kim [c]

[a] Department of Physics, Pukyong National University, Busan 608-737, South Korea
[b] Department of Physics, Changchun Normal University, Changchun 130032, China
[c] School of Materials Science and Engineering, Pusan National University, Busan 609-735, South Korea

ARTICLE INFO

Article history:
Received 7 July 2010
Received in revised form
28 October 2010
Accepted 8 November 2010
Available online 21 November 2010

Keywords:
CeF_3:Tb^{3+}
Nanocrystals
PL

ABSTRACT

CeF_3 and CeF_3:Tb^{3+} nanocrystals were successfully synthesized through a facile and effective polyol-mediated route with ethylene glycol (EG) as solvent. Various experimental techniques including X-ray diffraction (XRD), field emission scanning electron microscopy (FE-SEM), and photoluminescence (PL) spectra as well as decay dynamics were used to characterize the samples. The results indicated that the content of NH_4F and reactant concentrations were key factors in the product shape and size. Excessive NH_4F was necessary for the formation of hexagonal nanoplates. The specific morphology of product can be controlled by changing the NH_4F content and reactant concentrations. In addition, Tb^{3+} doped-CeF_3 sample shows strong green emission centered at 544 nm corresponding to the $^5D_4$–$^7F_5$ transition of Tb^{3+}. Due to the decrease of nonradiative decay rate, the lifetime of $^5D_4$ level of Tb^{3+} become longer gradually upon increasing the size of product.

1. Introduction

Recent years have seen considerable attention in the development of inorganic luminescent nanocrystals (NCs) due to their many potential applications such as light emitting devices, optical amplifiers, biolabels, lowthreshold lasers, and so forth [1,2]. Among various luminescent materials, rare earth (RE) doped materials with nanoscale have stimulated more intense research interest because of their unique optical, catalytic, and magnetic properties [3,4]. Dramatic efforts have been dedicated to its design and synthesis. To date, RE doped NCs with various shapes, including zero-dimension (0D) isotropic nanoparticles [5]; 1D rods, wires, tubes, and belts [6,7]; two-dimension (2D) plate, disk, and sheet [8]; and hierarchical architectures such as nanoflowers [9], whisk-broom [10], and shuttle-shaped [11] have been reported. It has been demonstrated that the chemical and physical properties of nanoscale regime materials are strongly related to their morphology, dimensionality, and size [12–14]. It is expected to control and manipulate the physical and chemical properties of materials and therefore controlled fabrication ability is a challenging issue. To synthesize NCs with uniform size and shape is both scientifically and technically important.

Compared with the conventional oxide-based systems, RE fluorides possess advantageous properties as fluorescent host materials such as low vibrational energies, and the subsequent minimization of the quenching of the excited state of the RE ion [15,16]. Furthermore, they exhibit high ionicity, electron-acceptor behavior, high resistivity as well as adequate thermal and environmental stability and therefore are considered as ideal host materials for luminescent RE ions. As an important inorganic scintillator laser material, CeF_3 is a luminescent material with 100% activator concentration [17,18]. Bulk CeF_3 crystal possesses a hexagonal phase structure with a space group of $P3c1$ (D^4_{3d}), there are six molecules in the unit cell and lattice constants $a=7.13$ Å, $c=7.29$ Å. The Ce^{3+} ion in the CeF_3 crystal is coordinated by nine F^- and has a C_2 site symmetry [18]. So far, CeF_3 nanomaterials have been prepared via various wet chemical methods such as micromulsion method [19], hydrothermal method [20], liquid–solid–solution (LSS) procedure [21], and solvothermal methods [22], and so forth [9,23]. Among the previous researches on synthesis of CeF_3 NCs, particle and plate are of the two main shapes in which the product can adapt to form. Agglomerated nanoparticles with a 15–20 nm diameter were obtained by micromulsion method [19]; round nanoplates were produced by a hydrothermal method using NaF as the fluoride source [20]; oil-soluble CeF_3 nanoparticles with a 6–15 nm diameter were synthesized by LSS approach [21], which is a new method and favor the control on the size and monodisperisity; polyol route employed by Wang et al. [22] only yielded agglomerated nanoparticles rather than the regular hexagonal

* Corresponding author.
E-mail address: jhjeong@pknu.ac.kr (J.H. Jeong).

0022-4596/$ - see front matter © 2010 Elsevier Inc. All rights reserved.
doi:10.1016/j.jssc.2010.11.015

nanoplates reported herein. Nanodisks, rods, and dots were produced by a mild ultrasound assisted route in an aqueous solution [23]. Very recently, flowerlike CeF_3 nanostructures were collected via a microwave irradiation route [9].

In this work, we present a general polyol synthesis of fluoride nanomaterials: 0D particles and 2D nanoplates CeF_3 and CeF_3:Tb^{3+}. The influence of the reactants concentration, and ratio of reactant on the morphology and size of the final products are studied. In addition, the photoluminescent (PL) properties of as-prepared samples with different shape and size are also investigated.

2. Experimental

2.1. Sample preparation

All chemicals were of analytical grade and were used as received without further purification. In a typical procedure for the preparation of CeF_3 NCs, appropriate amounts of NH_4F (6, 16, 24, 32 mmol) was dissolved in 20 mL of ethylene glycol (EG). Afterward, a solution of 2 mmol $Ce(NO_3)_3 \cdot 6H_2O$ in 20 mL of EG was added into the above solution under vigorous stirring. After stirring for 30 min, the mixed solution was transferred into a Teflon bottle of 70 mL held in a stainless steel autoclave, sealed, and maintained at 180 °C for 48 h. As the autoclave was cooled to room temperature naturally, the precipitates were separated by centrifugation, washed with deionized water and ethanol in sequence, and then dried in air at 70 °C for 12 h.

CeF_3:Tb^{3+} (10 mol%) were prepared in the same procedures except for adding 1.8 mmol $Ce(NO_3)_3 \cdot 6H_2O$ and 0.2 mmol $Tb(NO_3)_3 \cdot 6H_2O$ instead of 2 mmol $Ce(NO_3)_3 \cdot 6H_2O$.

In our experiments, different samples have been synthesized to study the relationship between reaction condition and morphology of product. It should be pointed out that when the effect of a reaction condition was studied, the other reaction conditions were kept same as those for the typical synthesis.

2.2. Measurements and characterization

X-ray diffraction (XRD) patterns of the samples were obtained with a Philips XPert/MPD diffraction system with Cu$K\alpha_1$ radiation ($\lambda = 1.54056$ Å). Field emission scanning electron micrograph (FESEM) images were taken on a Hitachi S-4200 electron microscope. The visible emissions were collected using a photon technology international (PTI) fluorimeter using a Xe-arc lamp with a power of 60 W. The fluorescence lifetimes were measured using a phosphorimeter attachment to the main system with a Xe-flash lamp (25 W power) with a dominant excitation wavelength of 245 nm.

3. Result and discussion

3.1. Structure and morphology

Fig. 1 shows XRD patterns of CeF_3 sample (up) and the standard data for CeF_3 (down). According to the JCPDS standard card, the pattern is in good agreement with hexagonal phase structure (JCPDS Card 08-0045). In this paper, the samples synthesized with NH_4F contents of 6, 16, 24, and 36 mmol are denoted as S1, S2, S3, and S4, respectively. Noted that except for NH_4F contents, the other reactants including amount of rare earth ions and volume of EG were kept constant all the time. In Fig. 2, XRD patterns of S1–4 are presented. It can be seen that all four samples crystallize in the hexagonal structure. With increasing the NH_4F contents from 6 to 32 mmol (from the top to the bottom in Fig. 2), the XRD patterns become narrower and narrower, suggesting a gradually increased

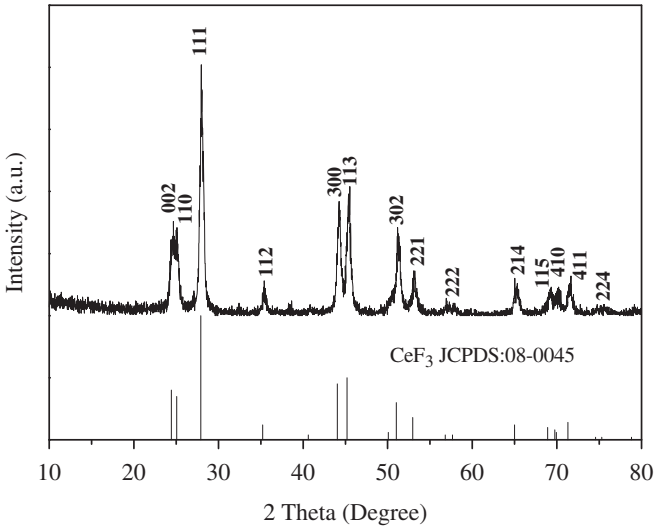

Fig. 1. XRD patterns of as-prepared CeF_3 samples. The line spectrum corresponds to the literature data of bulk CeF_3. (JCPDS no. 08-0045).

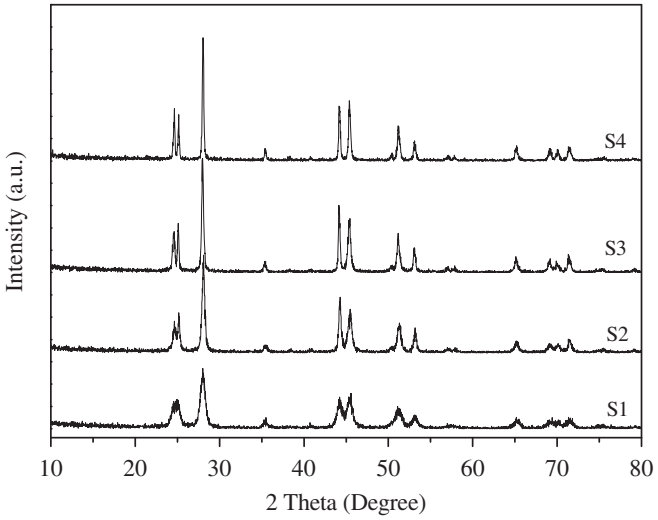

Fig. 2. XRD patterns of CeF_3:Tb^{3+} S1–4 obtained with different NH_4F content.

tendency of the crystallite size according to the Scherrer equation ($D = k\lambda/\beta\cos\theta$). Based on the XRD analysis, we can conclude that the NH_4F content play an important factor in controlling the size and crystallographical growth. The morphology of the as-prepared product is illustrated in Fig. 3. When the NH_4F content is stoichiometric, i.e., 6 mmol, sample is composed of ~35 nm nanoparticles which seems to be roughly spherical in shape (Fig. 3A). As the NH_4F content increases to 16 mmol, hexagonal 2D nanoplates appear although the shape is irregular (Fig. 3B). Upon further increasing the content of NH_4F to 24 and 32 mmol, the shape of the nanoplates become more and more regular and the size of the nanoplates become bigger and bigger. The average diameters are 65, 140, and 210 nm and the average thicknesses are 20, 40, and 70 nm, corresponding to samples S2, S3 and S4, respectively. This result demonstrates that excessive NH_4F was necessary for the formation of hexagonal nanoplates, and the shape of nanoplates becomes more regular as increasing the NH_4F content. As shown recently, the anisotropic nature of building block in crystal structure of NCs, the selective adsorption of surfactant onto specific crystal planes as well as the balance between the kinetic and thermodynamic growth regimes in solutions is three

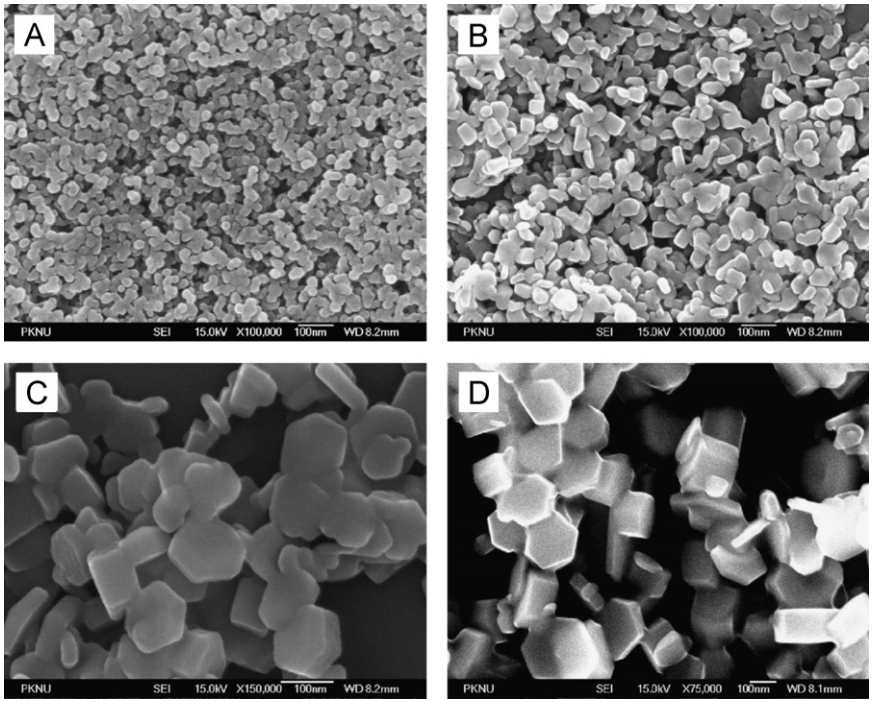

Fig. 3. FE-SEM images of CeF_3:Tb^{3+} samples: (A) S1, (B) S2, (C) S3, and (D) S4.

major driving forces for the crystal shape control of inorganic NCs [24,25]. Herein, the hexagonal CeF_3 seeds have anisotropic unit cell structures, which can induce preferential growth along crystallographically reactive directions. In addition, the increase of monomer concentration can significantly enhance the crystallization speed when the reaction was performed at high NH_4F/RE ratios. Previously reports [24–28] have shown that accelerated crystallization process related to the high monomer concentrations is another main driving force for anisotropic growth of inorganic nanostructures, which is beneficial for growing well-crystallized and regular-shaped NCs. As seen in the FESEM results of Fig. 3, our study follows well this viewpoint, where when the NH_4F/RE ratio was around the stoichiometric value, only irregular spherical nanoparticles appeared due to low monomer concentration; when the NH_4F/RE ratio was high enough, more regular and uniform hexagonal-shaped nanoplates were observed. The results further supported the monomer concentration-controlled kinetic model.

Furthermore, it can be seen (Fig. 3) that, the aspect ratio T/D (thickness/diameter) in the 2D nanoplates has no obvious variation, the values are 0.31, 0.29, and 0.30 for samples S2–S4, respectively. In principle, crystal growth and morphology are governed by the degree of supersaturation, the diffusion of the reactant species to the surface of the crystals, the surface and interfacial energy, and the structure of the crystals; that is the crystal structure, and the growth surroundings [29,30]. For the aspect ratio T/D, it is mechanistically determined by the relative rates of growth along different crystallographic directions. In general, faces perpendicular to the fast directions of growth have smaller surface areas, and slow growing faces therefore dominate the final morphology [30]. For NCs with a hexagonal crystal structure and hexagonal plate shape, the surfaces are typically {0001} for top/bottom planes and a family of six energetically equivalent $\{10\bar{1}0\}$ side planes ($(10\bar{1}0)$, $(\bar{1}010)$, $(0\bar{1}10)$, $(01\bar{1}0)$, $(1\bar{1}00)$, and $(\bar{1}100)$) on the basis of the known or similar models [31]. In the present work, the surface energy of $\{10\bar{1}0\}$side planes may be much higher than that of {0001} top/bottom planes considering that CeF_3 nanoplates preferentially extend along the former directions over the whole growth process. With regard to the unchanged T/D, we consider that the relative rates of growth along the {0001} and $\{10\bar{1}0\}$ face show no obvious change with increasing the content of NH_4F. As well documented in some literatures, influence of F^-concentration on size and shape of samples have been previously investigated in other RE fluorides such as LaF_3 and $NaYF_4$. Qin et al. [32] synthesized hexagonal LaF_3 through a polyol route using NH_4F as F-source and found that excessive NH_4F can capped on the {0001} crystal surfaces of LaF_3 NCs and lead to the anisotropic growth and the aspect ratio evolution of product. Similarly, this phenomenon was also observed by Li et al. [33] in the preparation of hexagonal-shaped $NaYF_4$ microcrystals using NaF and YCl_3 as raw materials by varying NaF to Y^{3+} ratio. By contrast, it is suggested that preferential adsorption of F^- on some nanocrystal facets of CeF_3 be less important in present solvothermal systems, which may be related to the change of crystallographic structure and surface charge of NCs.

The effect of reactant concentration on morphology and size is also investigated. In this paper, we take the ratio of NH_4F to RE ion as 16 as an example and fix the volume of EG (40 mL) to synthesize samples. Three concentrations (NH_4F/RE: 16 mmol/1 mmol, 32 mmol/2 mmol, and 48 mmol/3 mmol) were selected and the samples are denoted as samples C1–C3, respectively. Fig. 4 shows the XRD patterns and SEM images of sample C1–3. XRD patterns revealed that three samples adopted a hexagonal CeF_3 structure and the crystallinity became better and better with the increase in concentration. It is pointed out that there is some difference from each other in the relative intensity for (002), (110), (111), (300) and (113) reflections, especially the intensity of (111) reflection relative to the others increased noticeably in C3 sample, which may imply the shape anisotropy and/or preferred growth along (111) orientation with higher reactant concentration. From the SEM images, it can be observed that all of three samples were characterized by hexagonal-shaped nanoplates but the size decreased from samples C3 to C1. The average diameters are 75, 210, and 300 nm and the average thicknesses are 25, 70, and 180 nm, corresponding to samples C1–C3, respectively. It indicates that the lower reactant concentration results in fewer monomers for the growth of CeF_3 nanoplates, which showed size shrinkage via the "defocusing" way [34].

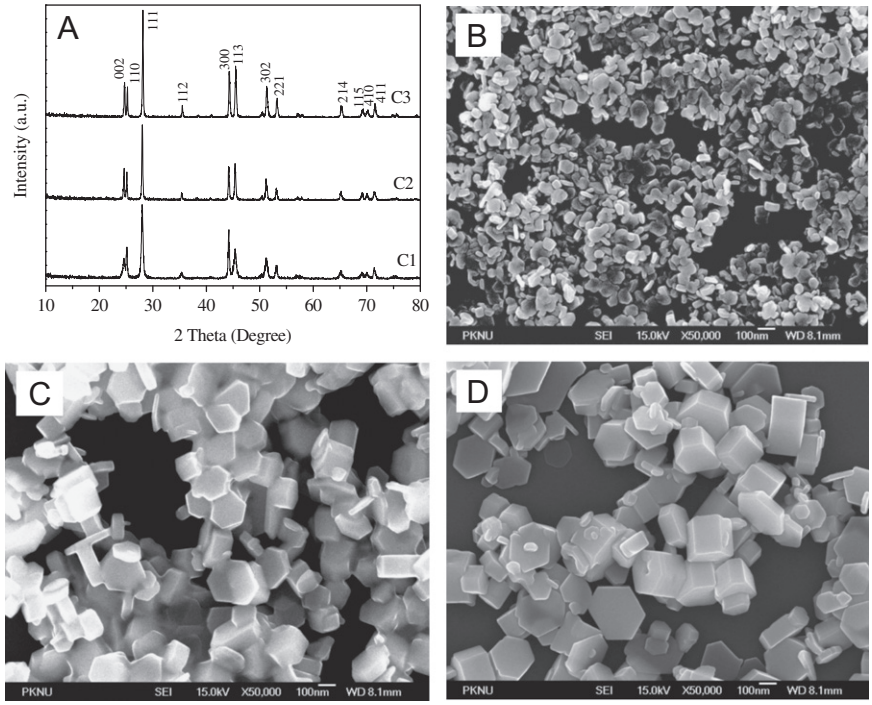

Fig. 4. (A) XRD patterns of the CeF_3:Tb^{3+} samples with different reactants concentration. (B) and (C) FE-SEM images of CeF_3:Tb^{3+} samples corresponding to the above XRD result. (B) C1, (C) C2, and (D) C3.

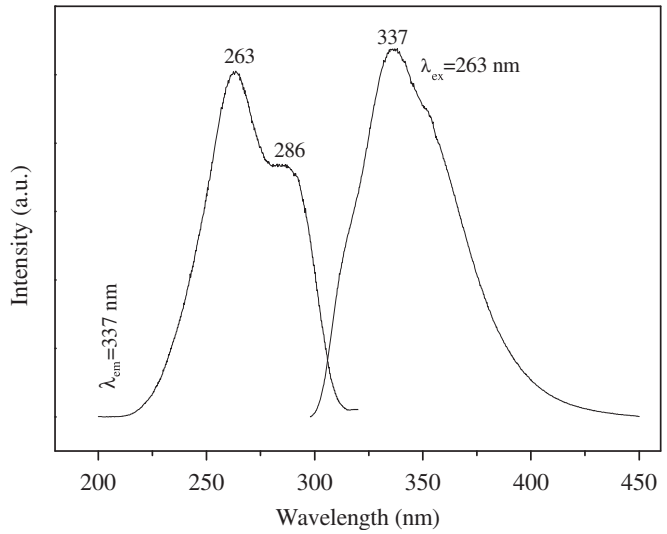

Fig. 5. Excitation (left) and emission (right) spectra of CeF_3 sample.

3.2. Excitation and emission spectra

CeF_3 sample shows an emission in the UV region. Fig. 5 gives the excitation (left) and emission (right) spectra of CeF_3 nanoplates. The emission spectrum of CeF_3 nanoplates includes a broad band ranging from 300 to 450 nm peaking at 337 nm, which can be attributed to the 5*d*–4*f* transition of Ce^{3+} [19,20]. Note that the profile of the spectrum is non-symmetrical, and should be contributed by different components. It has been reported that two well-resolved emission peaks were observed in the bulk [35] and nanowires [36] of $LaPO_4$:Ce^{3+} due to the ground-state splitting of Ce^{3+} ($^2F_{5/2}$, $^2F_{7/2}$). In the present CeF_3 nanoparticles the splitting for Ce^{3+} cannot be resolved clearly due to the broadening of spectral lines induced by the small size effects [22]. Monitored with the emission wavelength of 337 nm, the obtained excitation spectrum consists of two broad bands with maxima at 263 and 286 nm, which are associated with allowed 5*d*–4*f* transitions from the ground state $^2F_{5/2}$ of Ce^{3+} to different crystal field components of 5*d* levels split by the crystal field [22,23,37].

As the CeF_3 NCs are doped with Tb^{3+} ions, they exhibit strong green luminescence under UV excitation. Fig. 6 shows the excitation (A) and emission (B) spectra of sample S1–4. It can be seen that excitation spectrum (Fig. 6A) monitored with the 544 nm emission ($^5D_4$–$^7F_5$) of Tb^{3+}, including a strong allowed 4*f*–5*d* transitions of Ce^{3+}, is almost identical to that of pure CeF_3 nanoparticles (Fig. 5) except that a weak forbidden *f*–*f* transitions of Tb^{3+} ions in the UV range, which were associated with $^7F_6$–$^5D_3$, $^7F_6$–^5G_J, and $^7F_6$–$^5L_6$ transitions of Tb^{3+}. Note that the above broad band should include the contribution from Tb^{3+} ions given the case that Tb^{3+} ion also suffers from the 4*f*–5*d* transition in the spectral range above 300 nm. Actually, we measured the excitation spectrum of bulk TbF_3 (not shown here), however, 4*f*–5*d* transitions are usually weaker than its *f*–*f* transitions and narrower than that of Ce^{3+}, like those demonstrated in YPO_4:Ce^{3+} and YPO_4:Tb^{3+} [38]. In addition, the 5*f*–4*d* transition bands of Ce^{3+} ion in four samples show a little variation, the bands are located at 260.5, 286, 272.5 and 266.5 nm, respectively, in the samples S1–4. Particularly for the nanoplates, the reduced size from S4 to S2 was companied by the red shift of excitation peak. These results may be related to the variations of $^5d_1$ excited state of Ce^{3+} in different samples. The $^5d_1$ excited electronic configuration of Ce^{3+} is not shielded from the surroundings and is very sensitive to the change surrounding Ce^{3+} ions at or near the surface [36], which may descend when the grain size becomes smaller and lead to a red shift in the excitation spectra [39]. However, with smaller size, the nanoparticles (sample S1) do not follow the above trend to red shift further, which may be related to the difference in shape. The shape-dependent luminescence properties have been observed previously in CeF_3 and CeF_3:Tb^{3+} NCs [23].

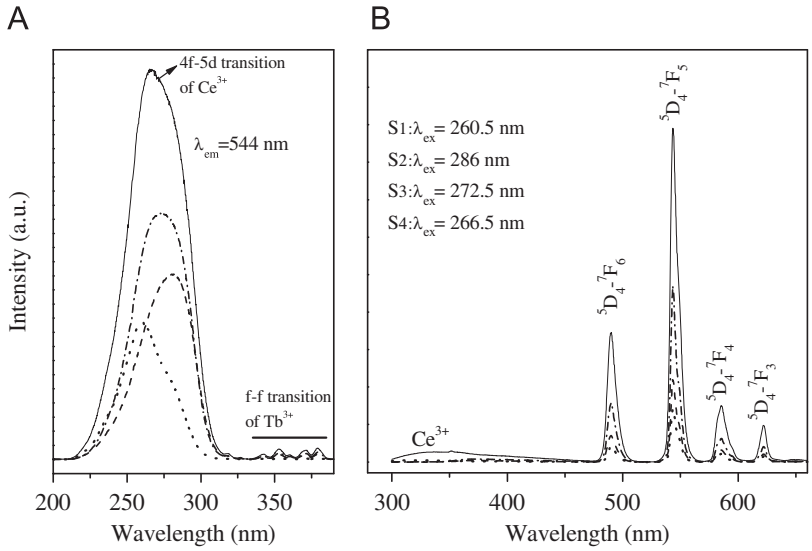

Fig. 6. Excitation (A) and emission (B) spectra of CeF_3:Tb^{3+} upon excitation into the Ce^{3+} absorption bands at 260.5, 286, 272.5 and 266.5 nm in the samples S1–4, respectively. S1: dot line; S2: dash line; S3: dash dot line; and S4: solid line.

In Fig. 6B, a weak emission of Ce^{3+} and a strong emission of Tb^{3+} ion can be both observed upon excitation into the Ce^{3+} absorption bands at 260.5, 286, 272.5 and 266.5 nm in the samples S1–4, respectively. The green emission is due to transitions from the excited $^5D_4$ level to the ^7F_J (J=3–6) ground states of Tb^{3+} ions, which was labeled in Fig. 6B. This result indicates that an effective energy transfer process from Ce^{3+} to Tb^{3+} occurs in CeF_3:Tb^{3+} samples [22,23,37,40]. That is, the Ce^{3+} acted as a sensitizer which absorbed UV light first and then transferred the energy to Tb^{3+} acceptor in the time scale of picosecond or faster, and then nonradiatively relaxes to the excited ^5D_J levels, yielding visible fluorescence. As discussed above, although self-excitation of Tb^{3+} ions through the 4*f*–5*d* and *f*–*f* transition absorption can also produce the green emission; however, the emission intensity should be two orders of magnitude weaker than that via Ce^{3+}–Tb^{3+} energy transfer route due to an inherent low excitation efficiency. Thereby, the strong green emission observed currently should mainly originate from the Ce^{3+}–Tb^{3+} energy transfer process. It is well known that Tb^{3+} has a relatively simple 4*f*-configurational energy level structure: low-energy states ^7F_J (J=6, 5, 4, 3, 2, 1, 0) and emitting levels of $^5D_3$ and $^5D_4$. In general, the blue luminescence from the transitions of $^5D_3$ to ^7F_J dominates emission spectra with a very low concentration of Tb^{3+} doped into host matrix. With increasing Tb^{3+} concentration, the cross-relaxation from $^5D_3$ to $^5D_4$ occurs due to the interaction between the neighboring Tb^{3+} ions, which increases accordingly the population of $^5D_4$ energy level. In consequence, green-light emitting from the transitions of $^5D_4$ to ^7F_J becomes dominant in the visible spectrum range [37]. In this work, there is no emission from higher level ($^5D_3$) observed because of the cross-relaxation phenomenon at the present high doped concentration of Tb^{3+} ion (10 mol%) [37,41]. The blue emission of the $^5D_3$–^7F_J transition is also difficult to be observed in other Ce^{3+} and Tb^{3+} co-doped system such as $LaPO_4$/Ce^{3+}, Tb^{3+}.

3.3. PL decay dynamics

The room-temperature luminescent dynamics were also measured. Fig. 7 shows the luminescent decay curves of S1–4 by monitoring the emission of Tb^{3+} at 544 nm. It can be seen that all of the four curves can well fit with a single-exponential function as $I=I_0\exp(-t/\tau)$ (τ is 1/*e* lifetime of the Tb^{3+} ion). In general, a

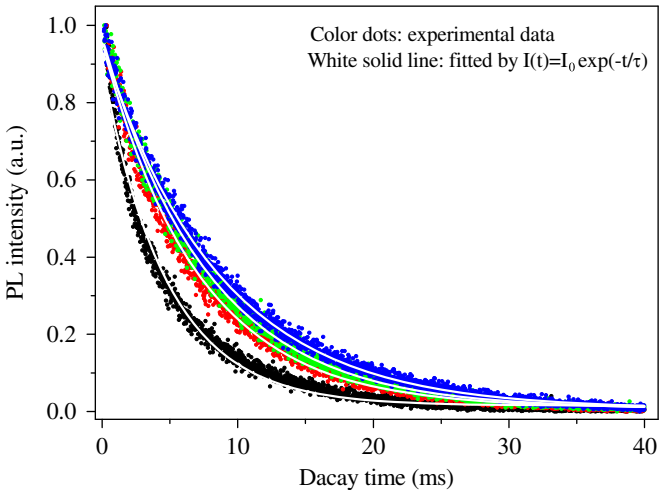

Fig. 7. Luminescence decay curves from $^5D_4$ level of Tb^{3+} in CeF_3:Tb^{3+} NCs upon excitation into the Ce^{3+} absorption bands at 260.5, 286, 272.5 and 266.5 nm in the samples S1–4, respectively. S1: black dots; S2: red dots; S3: green dots; and S4: blue dots. (For interpretation of the references to colour in this figure legend, the reader is referred to the web version of this article.).

non-single-exponential decay behavior was frequently observed in energy-transfer assisted luminescence route [42].Whereas in the Ce^{3+}–Tb^{3+} energy transfer induced luminescence single-exponential function can usually be used well to fit the luminescence decay of energy acceptor of Tb^{3+} [22,23,38]. The lifetime is, respectively, determined to be 4.75, 7.07, 7.77 and 8.62 ms for the samples S1–4, that is, the value of lifetime increases gradually in the sequence from S1 to 4. Generally, the luminescence lifetime of $^5D_4$ level of Tb^{3+} is in the order of millisecond magnitude. The above observation is similar to previous reports [22,23,37]. With respect to the increase of lifetime, we consider that it can be attributed to the change of nonradiative decay rate since the fluorescent lifetime (τ) is dominated by the radiative (W_r) and nonradiative (W_{nr}) transition rates, which can be written as $\tau=1/(W_r+W_{nr})$. As is well known, in the NCs, surface defects such as broken bonds/dangling bonds and a large number of surface adsorptions such as OH– and CO_2 bonds are generally involved. The surface defects may quickly trap the energy from both by excited Ce^{3+} prior to energy transfer

and excited levels of Tb^{3+} nonradiatively; such surface adsorption groups have large phonon energy and can act as nonradiative relaxation channels to bridge the emitting levels of Tb^{3+} and the ground states, both giving rise to an increase of nonradiative transition rate [43]. As stated above, samples S1–4 are synthesized with different condition and therefore exhibit different morphology and size. From samples S1 to S4, the size becomes larger gradually, as a result, the surface to volume ratio decreases and the surface contamination should be decreased, and the nonradiative relaxation rate therefore decrease and the lifetime become longer accordingly. The lifetime evolutions may support the remarkably enhanced green emission from S1 to S4 (see Fig. 6B) observed under the same measurement conditions. The present changes in photoluminescence intensity further indicate that luminescence properties of nanosized CeF_3:Tb^{3+} are sensitive to the shape, particle size, structural defects and surface chemistry of sample.

4. Conclusions

In summary, 0D nanoparticles and 2D nanoplates CeF_3 and CeF_3:Tb^{3+} have been successfully fabricated through a facile and effective polyol process. The content of NH_4F and reactant concentration plays a critical role in controlling the final morphology and size of the product. With low content of NH_4F, 0D nanoparticles were obtained. When the content of NH_4F exceeded a certain value, hexagonal and regular 2D nanoplates were formed. With increasing the content of NH_4F and reactant concentration the size of products increases. Furthermore, PL spectra showed that the CeF_3 and CeF_3:Tb^{3+} samples exhibited characteristic emissions of Ce^{3+} ($5d$–$4f$) and Tb^{3+} (f–f), respectively. The lifetime of Tb^{3+} in CeF_3:Tb^{3+} samples become longer with increasing the size of samples because the nonradiative processes at or near the surface of the nanomaterials are much reduced. The as-synthesized luminescent product may have some potential applications in the areas of light display.

Acknowledgments

This research was supported by Basic Science Research Program through the NRF funded by the Ministry of Education, Science and Technology (2009-0073255) and also this research was supported by National Core Research Center (NCRC) program through the National Research Foundation of Korea funded by the Ministry of Education, Science and Technology (2010-0001-226).

References

[1] K. Kompe, H. Borchert, J. Storz, A. Lobo, S. Adam, T. Moller, M. Haase., Angew. Chem. Int. Ed. *42* (2003) 5513–5516.
[2] G.A. Kumar, C.W. Chen, J. Ballato, R.E. Riman., Chem. Mater. 19 (2007) 1523–1528.
[3] X. Wang, Y. Li., Chem. Eur. J. 9 (2003) 5627–5635.
[4] B. Dubertret, P. Skourides, D.J. Norris, V. Noireaux, A.H. Brivanlou, A. Libchaber, Science 298 (2002) 1759–1762.
[5] H. Mai, Y. Zhang, R. Si, Z. Yan, L. Sun, L. You, C. Yan., J. Am. Chem. Soc. 128 (2006) 6426–6436.
[6] X. Bai, H. Song, G. Pan, Z. Liu, S. Lu, W. Di, X. Ren, Y. Lei, Q. Dai, L. Fan., Appl. Phys. Lett. 88 (2006) 143104.
[7] L. Wang, Y. Li., Chem. Mater. 19 (2007) 727–734.
[8] J.L. Lemyre, A.M. Ritcey, Chem. Mater. 17 (2005) 3040–3043.
[9] L. Ma, W. Chen, X. Xu, L. Xu, X. Ning, Mater. Lett. 64 (2010) 1559–1561.
[10] X. Xiao, B. Yan, Y. Song, Cryst. Growth Des. 9 (2003) 136–144.
[11] Z. Miao, Z. Liu, K. Ding, B. Han, S. Miao, G. An, Nanotechnology 18 (2007) 125605–12509.
[12] A.P. Alivisatas, Science 271 (1996) 933–937.
[13] Y.N. Xia, P.D. Yang, Y.G. Sun, Y.Y. Wu, B. Mayers, B. Gates, Y.D. Yin, F. Kim, H.Q. Yan, Adv. Mater. 15 (2003) 353–389.
[14] H.X. Mai, Y.W. Zhang, L.D. Sun, C.H. Yan., J. Phys. Chem. C 111 (2007) 13730–13739.
[15] P. Rahman, M. Green, Nanoscale 1 (2009) 214–224.
[16] J.H. Zeng, Z.H. Li, J. Su, L. Wang, R. Yan, Y. Li, Nanotechnology 17 (2006) 3549–3555.
[17] A.J. Wojtowicz, M. Balcerzyk, E. Berman, A. Lempicki, Phys. Rev. B 49 (1994) 14880–14894.
[18] K. Wei, C.X. Guo, J. Deng, C.S. Shi., J. Elec., Spectrosc. Relat. Phenom. A 79 (1996) 83–85.
[19] H. Lian, M. Zhang, J. Liu, Z. Ye, J. Yan, C. Shi., Chem. Phys. Lett. 395 (2004) 362–365.
[20] C. Li, X. Liu, P. Yang, C. Zhang, H. Lian, J. Lin., J. Phys. Chem. C 112 (2008) 2904–2910.
[21] X. Wang, J. Zhuang, Q. Peng, Y. Li., Inorg. Chem. 45 (2006) 6661–6665.
[22] Z.L. Wang, Z.W. Quan, P.Y. Jia, C.K. Lin, Y. Luo, Y. Chen, J. Fang, W. Zhou, C.J. O'Connor, J. Lin., Chem. Mater. 18 (2006) 2030–2037.
[23] L. Zhu, Q. Li, X.D. Liu, J.Y. Li, Y.F. Zhang, J. Meng, X.Q. Cao., J. Phys. Chem. C 111 (2007) 5898–5903.
[24] H.X. Mai, Y.W. Zhang, L.D. Sun, C.H. Yan, Chem. Mater. 19 (2007) 4514–4522.
[25] R. Si, Y.W. Zhang, H.P. Zhou, L.D. Sun, C.H. Yan., Chem. Mater. 19 (2007) 18–27.
[26] C.H. Liu, H. Wang, X. Li, D.P. Chen, J. Mater. Chem. 19 (2009) 3546–3553.
[27] C.H. Liu, H. Wang, X.R. Zhang, D.P. Chen., J. Mater. Chem. 19 (2009) 489–496.
[28] X.G. Peng, Adv. Mater. 15 (2003) 459–463.
[29] Q. Tang, W. Zhou, W. Zhang, S. Ou, K. Jiang, W. Yu, Y.T. Qian, Cryst. Growth Des. 5 (2005) 147–150.
[30] J. Yang, C.X. Li, Z.W. Quan, D.Y. Kong, X.M. Zhang, P.P. Yang, J. Lin, Cryst. Growth Des. 8 (2009) 695–699.
[31] C.X. Li, J. Yang, Z.W. Quan, P.P. Yang, D.Y. Kong, J. Lin, Chem. Mater. 19 (2007) 4933–4942.
[32] R. Qin, H. Song, G. Pan, X. Bai, B. Dong, S. Xie, L. Liu, Q. Dai, X. Qu, X. Ren, H. Zhao, Cryst. Growth Des. 9 (2009) 1750–1756.
[33] C. Li, C. Zhang, Z. Hou, L. Wang, Z.Q.H. Lian, J. Lin, J. Phys. Chem. C 113 (2009) 2332–2339.
[34] X. Peng, L. Manna, W. Yang, J. Wickham, E. Scher, A. Kadavanich, A.P. Alivisatos, Nature 404 (2000) 59–61.
[35] G. Blasse, A. Bril, J. Chem. Phys. 51 (1969) 3252–3254.
[36] L. Yu, H. Song, Z. Liu, L. Yang, S. Lu, Z. Zheng, J. Phys. Chem. B 109 (2005) 11450–11455.
[37] M. Yu, J. Lin, J. Fu, H.J. Zhang, Y.C. Han, J. Mater. Chem. 13 (2003) 1413–1419.
[38] H. Lai, A. Bao, Y. Yang, Y. Tao, H. Yang, Y. Zhang, L. Han, J. Phys. Chem. C 112 (2008) 282–286.
[39] H. Guo, Appl. Phys. B 84 (2006) 365–369.
[40] J.C. Bourcet, F.K. Fong, J. Chem. Phys. 60 (1974) 34–39.
[41] G. Blasse, B.C. Grabmaier, Luminescent Materials, Springer-Verlag, Berlin, Heidelberg, 1994.
[42] T. Fujii, K. Kodaira, O. Kawauchi, N. Tanaka, H. Yamashita, M. Anpo, J. Phys. Chem. B 101 (1997) 10631–10637.
[43] X. Qu, H. Song, G. Pan, X. Bai, B. Dong, H. Zhao, Q. Dai, H. Zhang, R. Qin, S. Lu, J. Phys. Chem. C 113 (2009) 5906–5911.